Using asymptotic methods to compute diffracted pressure by curved surfaces

Mikaël Vermet, Nicolas Noe, Rodolphe Vauzelle, Yannis Pousset, Pierre Combeau

Using asymptotic methods to compute diffracted pressure by curved surfaces.

Mikael Vermet, Nicolas Noé, Rodolphe Vauzelle, Yannis Pousset, Pierre Combeau

27 août 2009

1 Introduction.

This article presents an original and efficient method to compute acoustic pressure diffracted by curved surfaces. Our approach is perfectly suited to be integrated into ray of beam tracing softwares. First we will remind how diffraction by curved surfaces can be handled in asymptotic methods. Keller [1], stating on generalized Fermat' principle, established that the diffraction of an acoustic wave by a surface could be solved using creeping rays (fig 1). These creeping rays must hit the surface so as to be tangent with the surface (attachement point) and must leave it the same way (ejection point). Between these two points the ray must follow a geodesic on the surface (according to Fermat's principle). All these points are illustrated on figures 1(a) and 1(b).

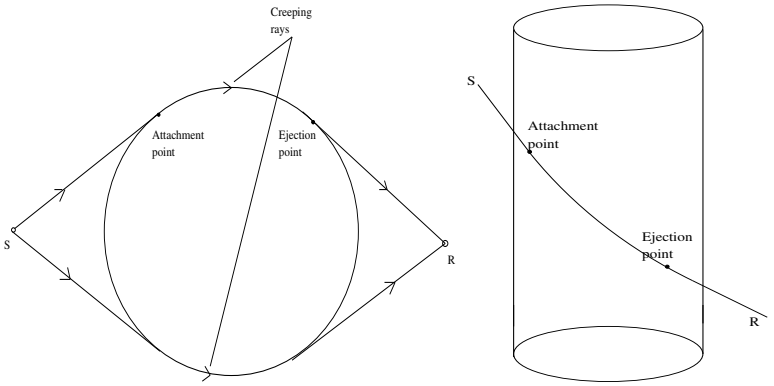

(a) Cross section view of rays creeping around a cylinder.

(b) Top view of rays creeping around a cylinder.

FIG. 1 – *Creeping rays needed to compute diffraction by the surface between source S and receiver R.*

Nevertheless integrating creeping waves computation in a ray or beam tracing code in order to solve complex problems is difficult. Indeed, the integration of creeping rays computation inside a global ray calculation can be very cumbersome. Moreover, almost all the complex surfaces available are originally discretized. As a consequence we decided to use a discretized approach, i.e. meshing our curved surfaces into triangles or quadrangles and to consider the creeping wave problem as a succession of diffractions by the straight edges separating these triangles or quadrangles (fig 2). Geodesics are then substituted by the intersection of the Keller cone with the meshed surface, at each diffraction edge. The reflection of rays on the curved surfaces is handled with a smoothed mesh of the surfaces, using linear interpolation of normals [2].

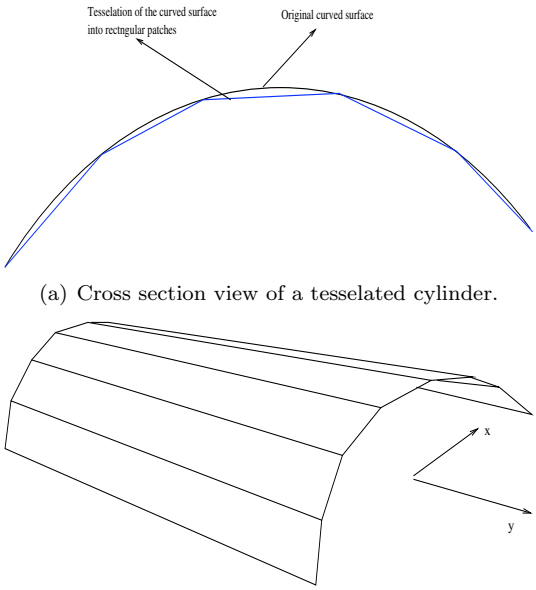

(a) Cross section view of a tesselated cylinder.

(b) Top view of a tesselated cylinder.

FIG. 2 – *Tesselation of the surface into rectangular patches.*

2 Implementation of the chosen method.

In order to handle successive diffractions in a ray-tracing environment we have to use asymptotic formula of diffraction coefficients. In [3] Kouyoumjian et Pathak treat multiple diffractions by multiplying the diffraction coefficients associated to each edge, and then apply a 1/2 factor for each edge on which incident waves grazes on the surface (for our case every edge will be applied this 1/2 factor). Unfortunately this approach fails, even for the simple case of a double diffraction by a wedge. It gives unsatisfying results in the transition region of the second edge and when edges are closer than 10 lambda. These two conditions (see figures 3(a) and 3(b)) are mandatory in our application to tesselated curved surfaces. We then chose to use Albani and Capolino formula [4, 5] that breaks through these limitations.

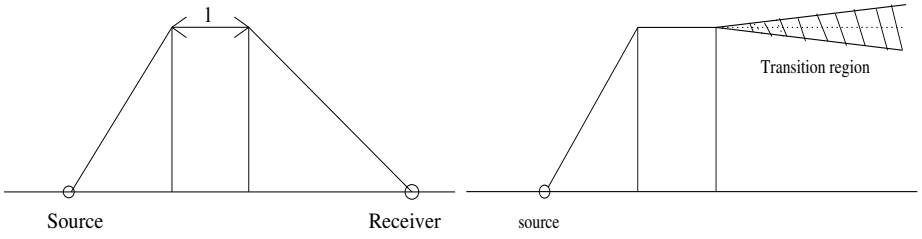

(a) Double wedge width is lower than a few wavelengths.

(b) The receiver is in the transition region of the second wedge case of failure of Pathak and Kouyoumjian formula.

FIG. 3 – *Situations in which Pathak and Kouyoumjian formula fails.*

Our approach is to handle successive edges two by two and to compute on each couple Albani and Capolino coefficients. When the number of diffractions is odd, the last one is computed using [3]. This is correct since Albani and Capolino formula enforces pressure continuity when the receiver lies in the transition region of the following even edge.

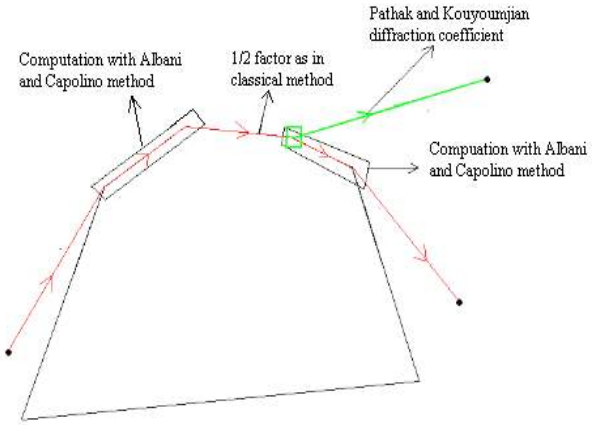

FIG. 4 – *Overview of our method to compute diffraction by a tesselated curved surface.*

2.1 Application to the case of a 2D cylinder.

We expose in this section the computation of acoustic diffraction by a cylinder with our method and compare it to reference results. The test configuration is displayed on fig. 5. The receivers are situated inside the rectangle delimited by the red lines. The cylinder is tesselated into 16 rectangular patches as illustrated in 2(b). Thus, the distance between two edges is about 1 wavelength at a 1 kHz frequency and 1/2 wavelength at a 2 kHz frequency. So this tesselation is sufficiently small because Albani and Capolino's formula gives good results above a 1/4 wavelength distance. The computation is performed in 2D, that is to say that the cylinder is infinite along the y axis. Moreover the wave is cylindric (lineic source). Our method is checked against a 2D BEM numerical [6] exact method. Indeed, the 2D BEM Method developed inside CSTB is able to treat cylinders without discretization. Moreover this configuration can be solved exactly with analytic asymptotic method (and so can be other analytic curved surfaces). Thus, we compare on figures 6 and 7 2D BEM results with asymptotic analytic solution of creeping waves found in [7], for a 1 kHz frequency. Thanks to this comparison we emphasize the efficiency of 2D BEM in treating exact cylinders. Indeed, we observe a good matching between the two results espescially in deep shadowing region where error is lower than 1 dB.

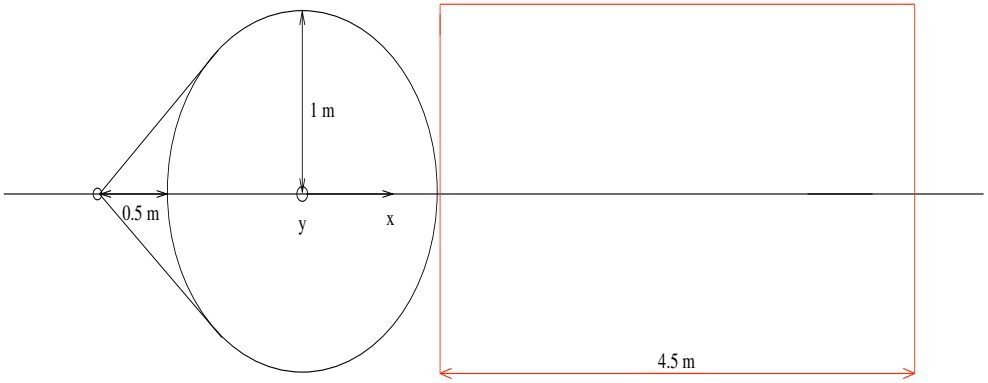

FIG. 5 – *First test case : 2D cylinder, cross section view.*

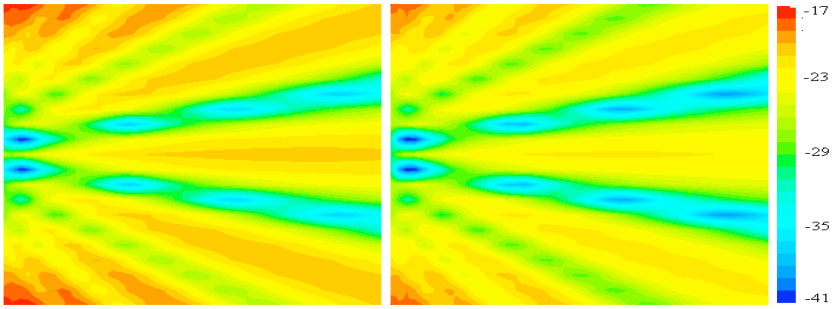

(a) 2D BEM results. (b) Asymptotic analytic results. (c) Scale (in dB).

FIG. 6 – *"Exact" methods results for a 2D cylinder.*

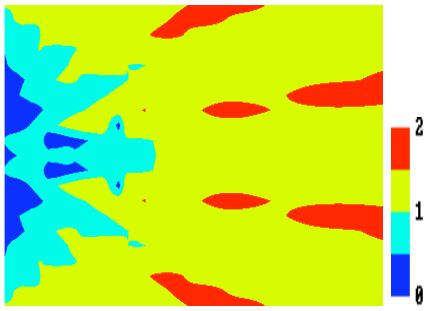

(a) Error between 2D BEM and asymptotic analytic results. (b) Scale (in dB).

FIG. 7 – *Error between "exact" methods for a 2D cylinder.*

Then we present on fig. 8 and 9 comparisons between 2D BEM and our method using beam-tracing [2] on a tesselated cylinder to find diffrated rays on the surface. Results are shown for 1 kHz and 2 kHz. There is very good matching between 2D BEM results and our method, espescially in deep shadow region where error is lower than 1 dB.

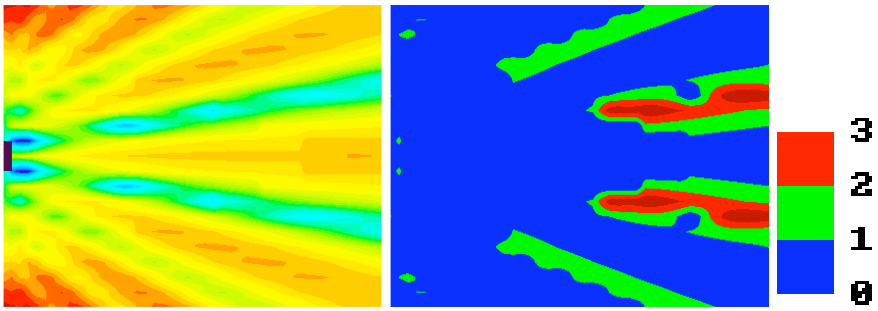

(a) Results with our method on a tesselated cylinder. (b) Error with 2D BEM results. (c) Scale (in dB).

FIG. 8 – *Error between 2D BEM results and our method using beam-tracing on a tesselated cylinder at 1 kHz.*

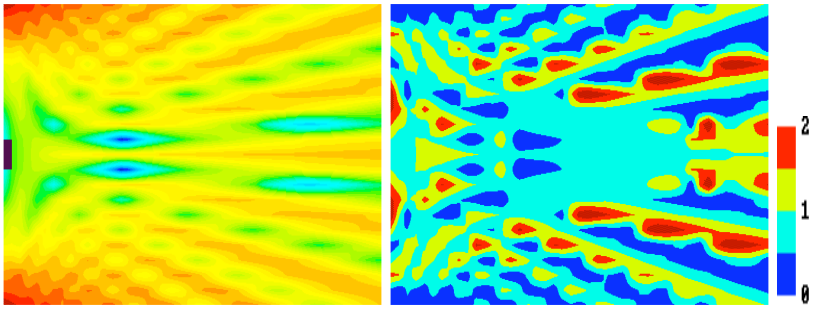

(a) Results with our method on a tesselated cylinder. (b) Error with 2D BEM results. (c) Scale (in dB).

FIG. 9 – *Error between 2D BEM results and our method using beam-tracing on a tesselated cylinder at 2 kHz.*

2.2 Open cylinder.

An open cylinder configuration is presented on figure 10. The cylinder is cut on ten degrees on each side of the x axis. Consequently the incident field from source S on points D and D' is first diffracted par straight edges on z axis at these points. These two points become then secondary sources on the cylinder.

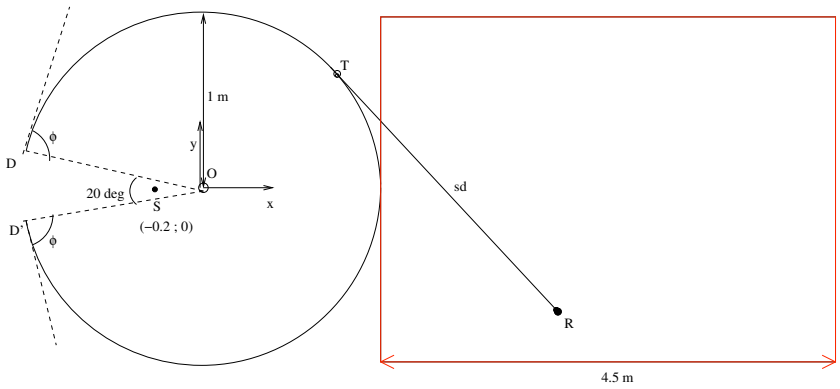

FIG. 10 – *Second test cas, 2D open cylinder.*

The analytical asymptotic solution of pressure at R is [8, 9] :

$$P(R) = \frac{e^{-jks'}}{s'} \cdot D_{GTD}(\phi) \cdot H \frac{e^{-jks_d}}{\sqrt{s_d}} \tag{1}$$

Where H is the Fock function.
We now present results from this analytical asymptotic solution compared to our beam-tracing computation result on a tesselated surface. We do not use 2D BEM here since an open cylinder is not a closed surface [6] (we would have to add thickness to the shape, leading to incoherent comparisons) that's why all the following validations are made with asymptotic analytical results. As for the full cylinder we tesselated the shape into 16 rectangular patches. Results are displayed on figures 11, 12 (1 kHz) and 13, 14 (2 kHz). We can observe on these figures a very good agreement between asymptotic analytical results and our beam-tracing results. The differences between acoustical levels calculated by these 2 methods at 1 kHz and 2 kHz are inferior to 1 dB on a large part of the receivers area.

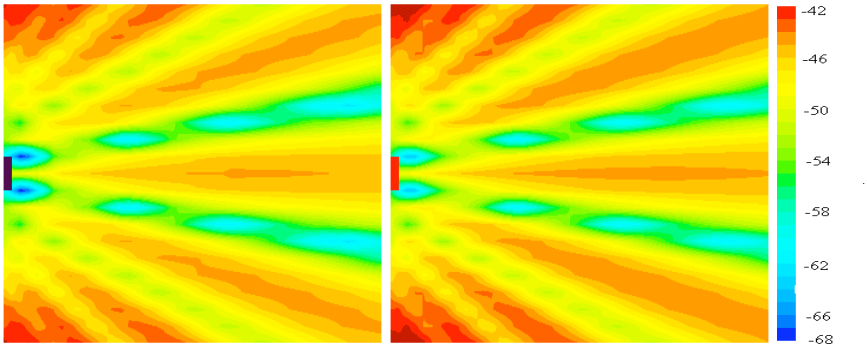

(a) Results with our method on a tesselated cylinder. (b) Results with analytical asymptotic method. (c) Scale (in dB).

FIG. 11 – *Results with our method and analytical asymptotic method on an open cylinder, 1 kHz.*

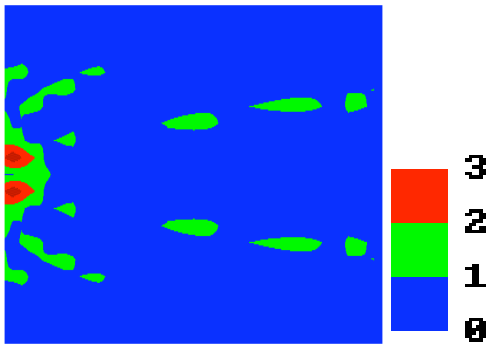

(a) Error between our method and analytical asymptotic method. (b) Scale (in dB)

FIG. 12 – *Error between our method and analytical asymptotic method, 1 kHz.*

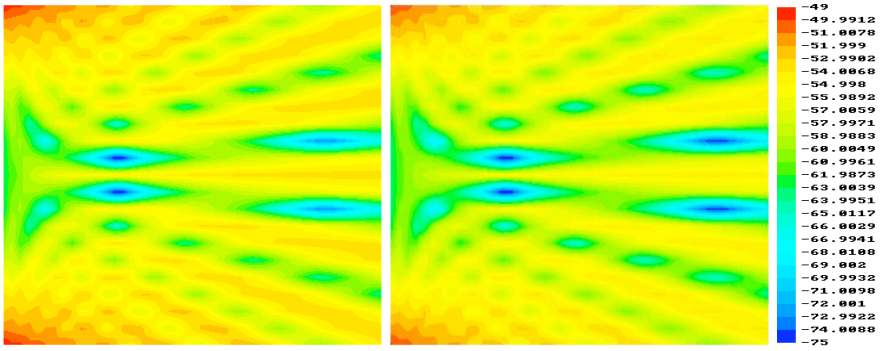

(a) Results with our method on a tesselated cylinder. (b) Results with analytical asymptotic method. (c) scale (in dB).

FIG. 13 – *Results with our method and analytical asymptotic method on an open cylinder, 2 kHz.*

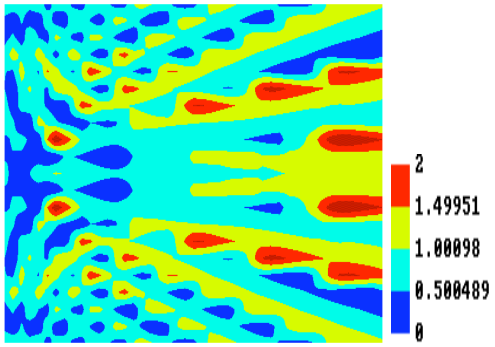

(a) Error between our method and analytical asymptotic method. (b) Scale (in dB).

FIG. 14 – *Error between our method and analytical asymptotic method, 2 kHz.*

2.3 A complete 3D test case.

We present in this section results for a complete 3D test case (figures 15) which is a part of a cylinder. This enables us to show that, when added with all the other contributions (diffractions by straight and ciruclar edges, reflexions,...), creeping waves contributions gives non negligible improvements to results accuracy and better agreement with exact numerical results.
The incident wave is now a spherical wave and the geometry is now limited in the y direction : hence part of circular edges that bound the surface will now diffract. All interactions (reflections on the source side, diffractions by straight and curved edges, creeping waves) are taken into account. Figure 16 is a 3D view of the geometry, source and receivers. Source position is [-1.4;0.7;-1.7] and is the red spot. Receivers are in a rectangle delimited by y = 0, x in [-1:4], z in [-3:3] and are the green dots.

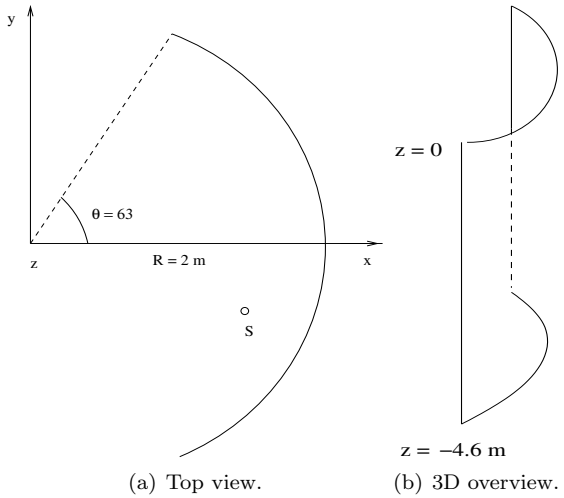

(a) Top view. (b) 3D overview.

FIG. 15 – *Overview of the 3D case.*

Figure 17 emphasizes the importance of the creeping waves in this particular test case. Figure 17(a) corresponds to a computation without creeping waves; reflections, diffractions by both vertical straight edges and diffractions by both top and bottom circular edges are taken into account. On figure 17(b) creeping waves are taken into account. Results shown on figure 17(c) has been obtained by 3D BEM. We

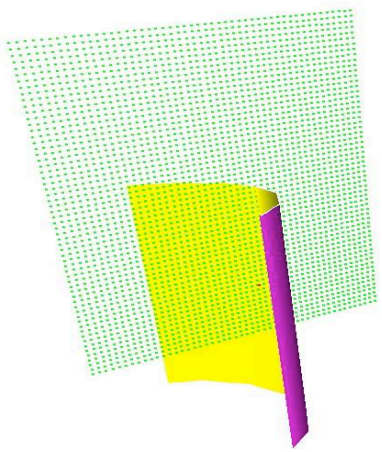

FIG. 16 – *3D test case with source and receivers .*

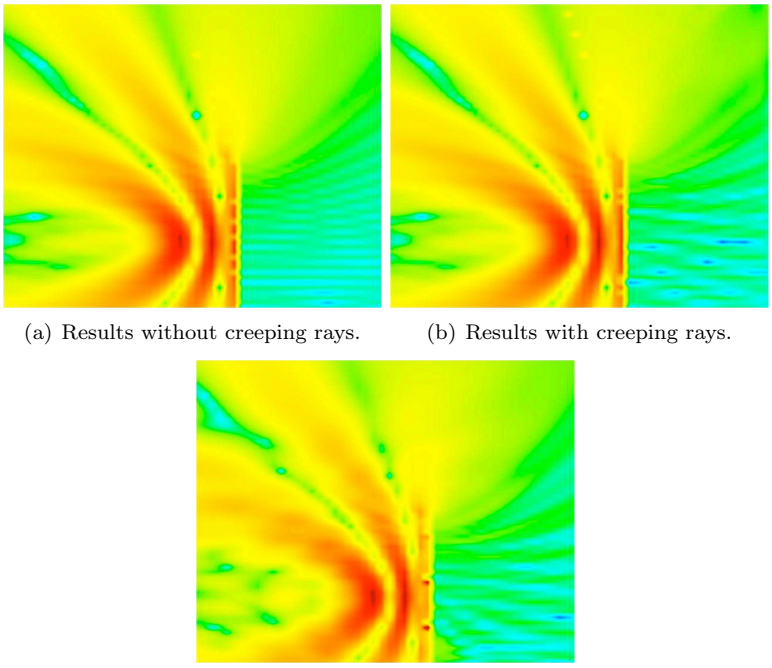

(a) Results without creeping rays. (b) Results with creeping rays.

(c) 3D BEM results.

FIG. 17 – *Comparison of beam-tracing results to 3D BEM reference on a part of cylinder: importance of creeping waves in the interference pattern.*

observe that in the inferior right part of figure 17(b) (correponding to the cylinder shadow region), creeping rays contributions considerably distort figure 17(a) and give a better agreement with 3D BEM results.

3 Conclusion

We have proposed through this paper an original method which is able to calculate creeping waves on tesselated curved surfaces. This last aspect is very important because in beam tracing applications, surfaces are very often discretized. Results

presented in this paper show a very good agreement between our approach and exact numerical methods. Moreover we emphasize the improvements provided by the creeping waves contributions concerning the pressure calculation accuracy when a complete 3D configuration has to be considered.

4 Annexe A : coefficient de double diffraction de Albani et Capolino.

We sumarize here Albani and Capolino formula used into our creeping rays diffraction method. A 1/2 factor is added to the original formula since the incident ray on edge E3 is grazing. We define respectively distances between edges E2 and E3, between E3 and E4, E4 and receiver R as : r_1, l, r_2. $n_1\pi$ and $n_2\pi$ are the external wedges opening angles associated to the edges E3 and E4.ϕ_1 which is the incidence angle on edge E3 is equal to $n_1\pi$, while ϕ_2 corresponds to the angle between the diffracted ray and the face common to edges E3 and E4. Formula giving pressure

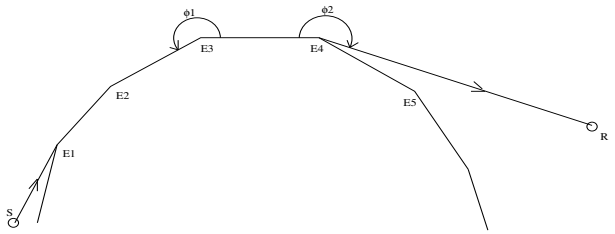

FIG. 18 – *Creeping rays needed to compute diffraction by the surface between source S and receiver R.*

at R is given by :

$$P(R) = \frac{e^{-jkr_1}}{r_1} \cdot A \cdot D_{12}^h \tag{2}$$

D_{12}^h is the double diffraction coefficient adaptated to edges E3 et E4.

$$A = \sqrt{\frac{r_1}{lr_2(r_1+l+r_2)}} e^{-jk(l+r_2)} \tag{3}$$

$$D_{12}^h = \frac{1}{4\pi jk} \sum_{p,q=0}^{2} \frac{(-1)^{p+q}}{n_1 n_2} \cot\left(\frac{\Phi_1^p}{2n_1}\right) \cot\left(\frac{\Phi_2^q}{2n_2}\right) T(a_p,b_q,w) \tag{4}$$

T is the transition function defined here.

$$T(a,b,w) = \frac{2\pi jab}{\sqrt{1-w^2}} \left\{ G\left(a, \frac{b+wa}{\sqrt{1-w^2}}\right) + G\left(b, \frac{a+wb}{\sqrt{1-w^2}}\right) + G\left(a, \frac{b-wa}{\sqrt{1-w^2}}\right) + G\left(b, \frac{a-wb}{\sqrt{1-w^2}}\right) \right\} \tag{5}$$

$$G(x,y) = \frac{y}{2\pi} e^{jt^2} \int_0^\infty \frac{e^{-jt^2}}{t^2+y^2} \mathrm{d}t \tag{6}$$

An asymptotical formula of this function is given in [10]. Formulas (7), (8), (9), (10) and (11) give us all the parameters involved in transition function T.

$$a_p = \sqrt{2k\frac{r_1 l}{r_1+l}} \sin\left(\frac{\Phi_1^p - 2n_1 N^p \pi}{2}\right) \tag{7}$$

$$b_q = \sqrt{2k\frac{r_2 l}{r_2 + l}} \sin\left(\frac{\Phi_2^q - 2n_2 N^q \pi}{2}\right) \tag{8}$$

$$w = \sqrt{\frac{r_1 r_2}{(r_1 + l)(r_2 + l)}} \tag{9}$$

$$\Phi_1^p = \phi_1 + (-1)^p \pi \tag{10}$$

$$\Phi_2^q = \phi_2 + (-1)^q \pi \tag{11}$$

N^p and N^q are the integers which verify the more closely the following relations :

$$2\pi n_1 N^p - \Phi_1^p = 0 \tag{12}$$

$$2\pi n_2 N^q - \Phi_2^p = 0 \tag{13}$$

Références

[1] J.B. Keller, Geometrical theory of diffraction, Journal of Optical Society of America. 52(1962) pp 116-130.

[2] N. Noé,

[3] P.H. Pathak, R.G. Kouyoumjian, A uniform geometrical theory of diffraction for an edge in a perfectly conducting surface, IEEE Transaction on antennas and propagation. 62(1974) pp 1448-1460.

[4] F. Capolino, M. Albani, S. Maci, R. Tiberio, Double diffraction at pair coplanar skewed edges, IEEE transactions on antennas and propagation. 45(1997), pp 1219-1226.

[5] F. Capolino, M. Albani, S. Maci, R. Tiberio, Diffraction at thick screen including corrugations top face, IEEE transactions on antennas and propagation. 45(1997) pp 277-283.

[6] P. Jean, A variationnal approach for outdoor sound propagation and application to railway noise, Journal of sound and vibration. 212(1998) pp 275-294.

[7] P.H. Pathak, An asymptotic analysis of the scattering of plane waves by a smooth convex cylinder, Radio Science. 14(1979) pp 419-435.

[8] P.H. Pathak, W.D. Burnside, R.J. Marhefka, A uniform GTD analysis of the diffraction of electromagnetic waves by a smooth convex surface, IEEE Transactions on antennas and propagation. 28 (5) (1980) pp 631-642.

[9] R.G. Kouyoumjian, P.H. Pathak, W.D. Burnside, Uniform GTD for diffraction by edges vertices convex surfaces, extrait de "Theoretical methods for determining the interaction of electromagnetic waves with structures", J.K. Skwirzinski. 1981.

[10] F. Capolino, S. Maci, Simplified closed form expressions for computing Fresnel integrals their application vertex diffraction, Microwave and optical technology letters. 9 (1995) pp 32-37.